# Guest–Host Interactions Investigated by Time-Resolved X-ray Spectroscopies and Scattering at MHz Rates: Solvation Dynamics and Photoinduced Spin Transition in Aqueous [Fe(bipy)3]2+

**ARTICLE** *in* THE JOURNAL OF PHYSICAL CHEMISTRY A · SEPTEMBER 2012

Impact Factor: 2.69 · DOI: 10.1021/jp306917x · Source: PubMed



**19 AUTHORS**, INCLUDING:

Wojciech Gawelda
European XFEL
**59** PUBLICATIONS **1,568** CITATIONS
SEE PROFILE

Elliot P Kanter
Argonne National Laboratory
**230** PUBLICATIONS **3,560** CITATIONS
SEE PROFILE

Tim Brandt Van Driel
Technical University of Denmark
**19** PUBLICATIONS **198** CITATIONS
SEE PROFILE

Henrik Till Lemke
Stanford University
**42** PUBLICATIONS **649** CITATIONS
SEE PROFILE

THE JOURNAL OF PHYSICAL CHEMISTRY A

Article

pubs.acs.org/JPCA

# Guest–Host Interactions Investigated by Time-Resolved X-ray Spectroscopies and Scattering at MHz Rates: Solvation Dynamics and Photoinduced Spin Transition in Aqueous $Fe(bipy)_3^{2+}$

K. Haldrup,[*,†] G. Vankó,[*,‡] W. Gawelda,[¶] A. Galler,[¶] G. Doumy,[§] A. M. March,[§] E. P. Kanter,[§] A. Bordage,[‡] A. Dohn,[∥] T. B. van Driel,[†] K. S. Kjær,[⊥] H. T. Lemke,[#] S. E. Canton,[▽] J. Uhlig, V. Sundström,[△] L. Young,[§] S. H. Southworth,[§] M. M. Nielsen,[†] and C. Bressler[¶]

[†]Centre for Molecular Movies, Department of Physics, Technical University of Denmark, DK-2800 Lyngby, Denmark

[‡]Wigner Research Centre for Physics, Hungarian Academy Sciences, H-1525 Budapest, POB 49, Hungary

[¶]European XFEL, Albert-Einstein Ring 19, D-22 761 Hamburg, Germany

[§]Argonne National Laboratory, 9700 South Cass Avenue, Argonne, Illinois 60439, United States

[∥]Chemistry Department, Danish Technical University, DK-2800 Lyngby, Denmark

[⊥]Centre for Molecular Movies, Niels Bohr Institute, University of Copenhagen, DK-2100 Copenhagen, Denmark

[#]Linac Coherent Light Source, SLAC National Accelerator Laboratory, Menlo Park, California 94025, United States

[▽]Department of Synchrotron Instrumentation and [△]Department of Chemical Physics, Lund University, Box 124, 22100 Lund, Sweden

**ABSTRACT:** We have studied the photoinduced low spin (LS) to high spin (HS) conversion of $[Fe(bipy)_3]^{2+}$ in aqueous solution. In a laser pump/X-ray probe synchrotron setup permitting simultaneous, time-resolved X-ray diffuse scattering (XDS) and X-ray spectroscopic measurements at a 3.26 MHz repetition rate, we observed the interplay between intramolecular dynamics and the intermolecular caging solvent response with better than 100 ps time resolution. On this time scale, the initial ultrafast spin transition and the associated intramolecular geometric structure changes are long completed, as is the solvent heating due to the initial energy dissipation from the excited HS molecule. Combining information from X-ray emission spectroscopy and scattering, the excitation fraction as well as the temperature and density changes of the solvent can be closely followed on the subnanosecond time scale of the HS lifetime, allowing the detection of an ultrafast change in bulk solvent density. An analysis approach directly utilizing the spectroscopic data in the XDS analysis effectively reduces the number of free parameters, and both combined permit extraction of information about the ultrafast structural dynamics of the caging solvent, in particular, a decrease in the number of water molecules in the first solvation shell is inferred, as predicted by recent theoretical work.

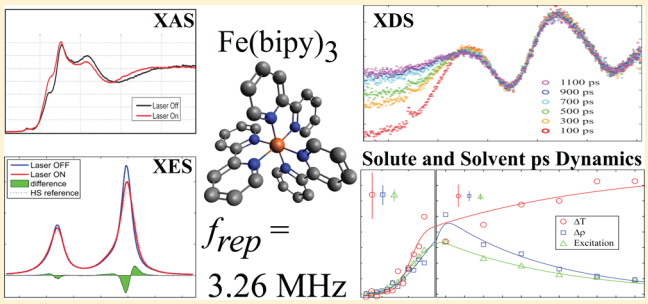


## INTRODUCTION

Chemical reactivity in the solution phase manifests itself often via a complex interplay between intramolecular processes of the parent molecule and guest–host interactions with the caging solvation shell. As a consequence, the influence of the solvent on the reactivity of chemical and biological species has been the subject of intense research over the past decades. Dynamic guest–host interactions are responsible for Stokes shifts between the absorption and emission spectra of excited molecules, which have been extensively studied by static and ultrafast optical studies.[1−3] Most studies for this purpose have focused on small molecules, where the close proximity to the solvent bath allowed extraction of substantial signals.[1,4] However, although, for example, ultrafast optical studies clearly show how fast the dynamics occur, the details of the structural rearrangement processes remained largely in the dark. Extending these studies to potentially functional systems, thus to larger molecules, has so far appeared unfeasible due to the expected small interaction between the central atom and the solvent host.

$[Fe(bipy)_3]^{2+}$ is a model compound for such functional systems as it can dynamically switch between a low spin (LS) ground to a high spin (HS) excited state upon illumination, starting via a metal to ligand charge transfer (MLCT) process, followed by an ultrafast back transfer within 130 fs, eventually undergoing a spin–flip to the HS state as well as a 0.2 Å

**Received:** July 12, 2012
**Revised:** September 11, 2012
**Published:** September 12, 2012

  

lengthening of the Fe−N bonds.[5,6] The bpy ligands are expected to effectively shield the central metal atom from the solvation shell, so that it appears impossible to extract any spectroscopic information on the solvation dynamics following the ultrafast LS−HS conversion. In order to investigate these dynamics, we have designed an ultrafast laser pump/X-ray probe experiment, where the probe exploits complementary structural tools to simultaneously reveal different details of the ongoing processes.

Time-resolved X-ray science on the ultrafast time scales is a young field aiming to deliver direct structural information with atomic-scale resolution about reaction intermediates during a light-triggered reaction. For such investigations, a UV−vis optical laser pulse serves as the pump source, and a time-delayed X-ray pulse serves as the probe. Most of the experimental methodology has been developed to an advanced state at synchrotron radiation sources over the past decade,[7−20] with the time resolution usually limited to ∼50−100 ps due to the intrinsic X-ray pulse width at synchrotrons, although the effective time resolution can be somewhat improved by a dense sampling of time points.[21,22] In nearly all cases, such studies on molecular systems have only employed X-ray absorption spectroscopy (XAS)[8,12,13,15−17,20,23−28] or X-ray scattering[7,9,11,14,18,19,21] techniques and have been, with few exceptions,[29] limited to rather low (1−2 kHz) pump/probe repetition rates, mainly due to the availability and constraints provided by chirped pulse amplifier (CPA) laser systems. In these experiments, a sufficient number of optical photons to match the number of ground-state molecules in the sample volume probed by the X-ray beam is available. In this way, photoexcitation of a large fraction of the sample (10−50%) can be obtained. However, due to the mismatch between the intrinsic (multi) MHz repetition rate of synchrotron sources and the kHz repetition rate of the CPA laser systems, the effective number of X-ray photons available for time-resolved measurements has remained several orders of magnitude lower than that actually delivered by conventional synchrotron sources. Experiments requiring significant X-ray flux such as nonresonant and resonant X-ray emission spectroscopies (XES) thus become very difficult to perform, although a recent breakthrough showed the first time-resolved XES experiment with picosecond time resolution using such a kHz laser system.[30] The results of that experiment demonstrated that the integrated number of X-ray probe photons is the bottleneck for using XES as a time-resolved X-ray technique, and consequently, it is highly desirable to increase the number of X-ray probe photons by better matching the repetition rates of the laser source to that of a synchrotron. The corresponding $10^3$ increase in effective X-ray flux would further allow many new applications within photochemical and photobiological dynamics,[31] where the low S/N for achievable and/or physiological concentrations has so far been a very significant limitation.

Only very recently and with the advent of high-power MHz laser systems have such photon-hungry experiments become feasible. So far, MHz laser pump/X-ray probe experiments have mainly been used in X-ray spectroscopy experiments,[32−34] and an extension to other X-ray tools is highly desired. In this paper, we report a study of the light-induced switching of the prototypical spin-crossover Fe(II) complex $[Fe(bipy)_3]^{2+}$ (see, e.g., ref 6 and references therein) at 3.26 MHz pump repetition rates with highly efficient use of the hard X-ray probe on the 10−100 ps time scale. The setup combines an emission spectrometer with absorption spectroscopy and includes a gateable area detector for collecting X-ray scattering data. This setup allows simultaneous acquisition of XES, XAS, and X-ray diffuse scattering (XDS) patterns. These complementary spectroscopic and scattering techniques are sensitive to, respectively, the spin state and configuration of the electron system and to the local and molecular structure and, in the case of XDS, include information about the solvent surrounding the complex. The complete setup thus allows full characterization of both electronic and geometric degrees of freedom simultaneously, as well as utilization of the full intensity of a third-generation synchrotron X-ray source in a time-resolved experiment. These advances in turn allow us to directly describe details of the solvent−solute dynamics previously only suggested by theory.

## EXPERIMENTAL METHODS

The X-ray microprobe capabilities[35] of beamline 7ID at Argonne National Laboratory's Advanced Photon Source (APS) and the experimental setup for ultrafast measurements at MHz repetition rates have previously been described in detail.[32] In the following sections, a brief overview will be presented, with particular focus on the experimental techniques and acquisition strategies employed in the present study.

**X-ray Spectroscopy.** X-ray absorption near-edge structure (XANES) spectroscopy relies on detecting modulations of the absorption cross section as a function of photon energy near an absorption edge. The absorption is dependent on both the local atomic configuration as well as the electronic configuration and the oxidation state of the absorber and thus provides information on the unoccupied electronic states, as well as the local molecular structure around the absorption center. Hence, the combination of electronic and structural changes can complicate interpretation, but the signal can be very intense, and the measurement is straightforward and employs either transmission detection or, as in the present setup, fluorescence detection.

By using, for example, a Bragg crystal spectrometer, the fine structure of the emitted X-ray fluorescence (individual emission lines) can be resolved. Such an XES spectrum stems from X-rays emitted when electrons fill in core holes; thus, this technique brings information about the occupied electronic states, information which is further enriched by the signatures of several key interactions (spin−orbit, multiplet, exchange) in the final state. The final states of XES are identical to those of photoemission spectroscopy; therefore, similar chemical sensitivity is observed.[36,37] The K$\alpha$ (1s2p) and K$\beta$ (1s3p) spectra of 3d transition-metal ions clearly reflect the 2p−3d and 3p−3d exchange interactions, respectively, which make the line shapes highly sensitive to the spin state.[38,39] (For the notations on X-ray transitions, see, for example, ref 40.) Owing to this, XES is more and more often used in spin state studies, particularly when there are advantages of working with penetrating hard X-rays, such as in high-pressure experiments.[41−43] When a transition involves two spin states, their distribution (the HS fraction, $\gamma$) can be readily and precisely calculated from the line shape variations.[39]

**Diffuse Scattering.** While the spectroscopic methods described above give accurate information on the electronic structure of the investigated systems, they are sensitive at best to the local structure around the absorber atom only, and they do not provide precise information about the full structural configuration of the other nuclei in the molecule under


dx.doi.org/10.1021/jp306917x | J. Phys. Chem. A 2012, 116, 9878−9887

investigation. This information is readily available from scattering studies, which probe the relative positions of the atomic nuclei by elastic scattering off (primarily) the associated core electrons in the entire sample.

In time-resolved studies utilizing X-ray Diffuse Scattering (XDS) from liquid samples, it is often beneficial to analyze the difference scattering signal $\Delta S \equiv S_{\mathrm{LaserOn}} - S_{\mathrm{LaserOff}}$, as this is a highly efficient way of suppressing the large static contribution to the scattering signal from the bulk solvent. By analyzing the difference signal, one studies the photoinduced changes triggered by the laser pump pulse only, typically a structural change in the solute coinciding with a (small) temperature increase of the solvent followed by subsequent bulk solvent expansion. These latter bulk solvent contributions to the difference signal can be readily determined in a separate experiment and can be robustly included in any structural analysis.[44]

As discussed in detail by Haldrup et al.,[45] the differenc scattering signal $\Delta S$ from solution state studies does not contain enough information to allow a direct structure determination. However, as has been established in previous time-resolved scattering studies, the information content is sufficient to allow quantitative model comparisons.[14,18,19,46−50] Within this approach, possible structural changes of an assumed initial structure are parametrized in terms of a few structural parameters, such as key bond lengths or angles. The best-fit or most-likely structure is then found by comparing simulated $\Delta S$ signals calculated from the putative structures of the solute molecules with the measured scattering signal. Such model comparisons are highly quantifiable[51] and can be implemented through both fast minimum searches[52] and full parameter-space mappings.[45] Both methods yield best-fit combinations of the model parameters, and the correlations between the parameters and parameter uncertainties can be estimated.

**Beamline Layout and Laser Setup.** Beamline 7ID is provided with X-ray photons from an APS type A undulator monochromatized by a double-crystal diamond monochromator. After focusing by Kirkpatrick−Baez mirrors, $2 \times 10^{12}$ ph/s ($3 \times 10^5$ ph/pulse in 24-bunch mode at a ring current of 102 mA) are delivered at a 10 keV energy to a sample spot size focused down to 5 $\mu$m (fwhm).[53]

The laser setup installed in the 7ID-D hutch is based on the high repetition rate Duetto system from Time-Bandwidth Products and is described in detail in the work by March et al.[32] This laser emits at a fundamental wavelength of 1064 nm with a repetition rate up to 6.52 MHz. The pulse width was chosen to be 10 ps. Focusing optics and an attenuator setup allow the fluence on the sample to be accurately controlled and can provide a 25 $\mu$m (fwhm) spot at the sample position. The spatial overlap between X-ray and laser pulses at the sample position is obtained by means of a motorized pinhole setup, and temporal overlap is achieved using a removable MSM (metal−semiconductor−metal) photodetector with a 30 ps rise time at the sample position. The spatial and temporal stability are 5 $\mu$m and 10 ps over several hours.[32] For all experiments reported in this work, the second harmonic at 532 nm was used to excite the sample, the pulse energy was 1.8 $\mu$J focused onto a $100 \times 80$ $\mu$m$^2$ fwhm spot, and the repetition rate of the laser was 3.26 MHz. For the XES/XDS measurements, a 7.5 keV monochromatic X-ray beam was focused to 7 $\mu$m × 8 $\mu$m and centered on the laser spot. The data shown in this work were acquired in two runs separated by only a few minutes. First, data from a laser/X-ray time delay of $\Delta t = -100$ to +1100 ps with 200 ps between time points were acquired; then, data from $\Delta t = -80$ to +30 ps with 10 ps between time points were acquired. Negative $\Delta t$ corresponds to the X-ray probe preceding the laser excitation pulse, and the total acquisition time was ∼12 h.

Figure 1 shows a schematic layout of the experimental setup. The laser and X-ray beams are almost collinear (5° crossing angle) and overlap on a fast-flowing 100 $\mu$m thick liquid jet mounted at 45$^{\mathrm{circ}}$ to the X-ray beam propagation direction. Lead foil with pinholes for the two beams is installed to limit air scattering, which is very significant at energies below 10 keV. In the horizontal plane and at right angles to the X-ray beam, X-ray emission detectors are installed, both a scintillator and a crystal spectrometer, and behind the sample, a Pilatus 100K area detector collects the forward-scattered X-rays. These detector systems for spectroscopy and scattering are described in further detail below.

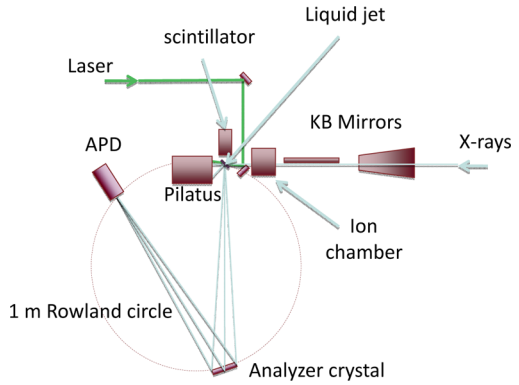


**Figure 1.** Experimental setup for the experiments reported here, seen from above. Laser and X-ray beams are focused and overlapped on a fast-flowing 100 $\mu$m thick sample sheet, and scattered X-rays are collected by a Pilatus 100K detector. The emitted X-ray photons are collected either directly by a scintillation detector for XANES using fluorescence detection or by an APD mounted in a 1 m Rowland circle dispersive setup within a He bag for XES measurements.

**XES Data Acquisition.** A wavelength-dispersive crystal spectrometer was constructed to measure the XES signal, with a spherically bent analyzer crystal of 10 cm diameter positioned at a 90° scattering angle and an avalanche photodiode (APD) detector at its focus, such that the sample−analyzer−detector setup constituted a 1 m Rowland circle. A thin plastic bag filled with He was installed around the spectrometer to minimize absorption losses. The spectra of the emitted X-rays were taken by scanning the Ge(440) and Si(531) spherically bent analyzer crystals through the appropriate Bragg angle range to collect the Fe K$\alpha$ and K$\beta$ spectra, respectively, and the APD was moved accordingly. For a particular time delay, two spectra were collected alternately, following the laser on/off pumping pattern. The total energy resolution measured through the spectrometer was 1.0 eV (fwhm) at 6404 eV, a resolution composed of 0.5 and 0.9 eV contributions from the beamline monochromator and the spectrometer, respectively.

**XDS Data Collection.** As described in detail by Ejdrup et al.,[54] the gated mode of the Pilatus detector is sufficiently fast to isolate single X-ray pulses from individual electron bunches with 153 ns spacing in the APS storage ring in 24-bunch mode. Combined with a synchronized laser system, this allows pump−probe studies with a time resolution determined by the width of the probe pulse, typically close to 80 ps in this mode.


dx.doi.org/10.1021/jp306917x | J. Phys. Chem. A 2012, 116, 9878−9887

To collect scattering data, a Pilatus 100K detector was placed 55 mm behind the sample. The detector plane was perpendicular to the X-ray beam direction and mounted with a horizontal offset to allow collection of scattered X-rays up to an angle of 53°. As the first step in the analysis, the direct beam and areas of the detector significantly affected by air scattering and by shadowing from the nozzle and beam stop mounts were masked out. Each image was then azimuthally integrated after applying appropriate geometric corrections.

The scattering data were collected in a sequential acquisition mode to allow robust construction of difference scattering signals $\Delta S$. For a given time delay, the laser pulses were synchronized to arrive $\Delta t$ before every other X-ray bunch from the synchrotron, giving an effective pump−probe repetition rate of 3.26 MHz. The gating signal to the Pilatus detector was then set to allow the scattering either from the laser-synchronized X-ray pulses or from the laser-off pulses to be detected and stored on the detector. The number of individual gating events per image acquisition was set to correspond to integration times of 5−10 s ($\sim 10^7$ gating events), leading to single-pixel photon counts of $\sim 10^5$ in the liquid peak. For each time delay, this sequence was then repeated until satisfying counting statistics for calculating $\Delta S$ with adequate signal-to-noise was reached, typically after 130 repetitions, corresponding to a total integration time of 40 min per time delay point for the best quality data. Choosing an energy of 7.5 keV, nearly 400 eV above the iron K-edge, this choice of integration time also allowed simultaneous collection of high-quality X-ray emission data.

A particular complication of the high-repetition-rate experiments in this and similar studies is that the sample volume investigated by a single pair of pump−probe pulses has already been previously subjected to a laser pump pulse. For setups conceptually similar to the one used here, this can be avoided up to repetition rates of ∼1 MHz using high-speed pump/jet systems (30 m/s) and small laser focus (<25 $\mu$m), but in the present case, the repetition frequency was significantly higher than the refresh rate of $f_{\text{refresh}} \approx 100$ kHz. For the X-ray spectroscopy data, this is not an issue as the lifetime of the photoexcited compound ($\tau$ = 665 ps[55]) is much less than the time between laser pulses (153 ns), effectively preventing multiphoton excitations from adjacent pump pulses. However, for the X-ray scattering studies, the changes in scattering due to the hydrodynamic evolution (heating followed by expansion) of the solvent need to be taken into account. For the experiments reported here, the contribution to the individual difference signals from previous pump events is common for all of the investigated time delays as the hydrodynamic evolution of the solvent is negligible on the single-nanosecond time scale after the first 100 ns following the impulsive heating event.[44] This contribution can therefore be readily determined by including a set of measurements where the laser pulse arrives shortly after the trailing edge of the X-ray pulse (e.g., $\Delta t = -100$ ps). This "background" difference signal can then be directly subtracted from the positive time delays to yield the difference scattering signal due only to the most-recent laser pulse, $\Delta S(\Delta t) = [S_{\text{On}}(\Delta t) - S_{\text{Off}}] - \Delta S_{\Delta t=-100\text{ ps}}$. All difference signals shown below have had the contribution from previous pump pulses removed by this background-subtraction method. This method is generally applicable for short-lived sample systems where the energy release to the solvent is fast compared to the 153 ns bunch spacing and where the solvent hydrodynamics evolve slowly after the first 100 ns. In cases where these requirements are not fully met, the determination of excitation fractions and quantitative discussions of the solvent response (e.g., a temperature increase) must adequately include the contributions from previous pump pulses.

## RESULTS AND DISCUSSION

**Spectroscopic Characterization of the HS State of $[Fe(bipy)_3]^{2+}$.** Figure 2 shows the XANES of $[Fe(bipy)_3]^{2+}$

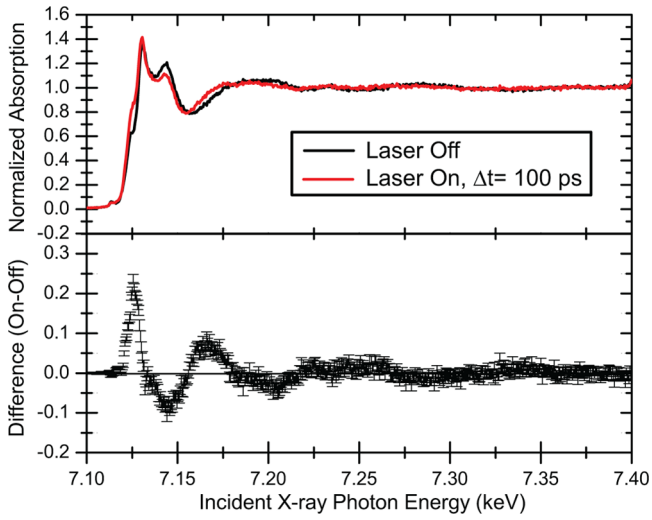


**Figure 2.** XANES spectra of a 20 mM aqueous solution of $[Fe(bipy)_3]^{2+}$, with and without laser excitation. The change from the LS to HS configuration is highly evident, and the S/N is observed to be excellent. XANES data were acquired in fluorescence-detection mode with a repetition frequency of 135.8 kHz.

before and 100 ps after the laser excitation, and the spectra are fully consistent with previous studies, indicating the light-induced formation of the HS state.[5,56] The S/N for both laser-on and laser-off measurements for this 135.8 kHz data acquisition are fully comparable to equivalent steady-state studies, highlighting the significant advantages of the high-repetition-rate schemes for time-resolved studies.

As described above, XES is a new probe in ultrafast experiments, and with a kHz repetition rate laser, it is at the limit of feasibility at synchrotron beamlines even at the most intense $K\alpha_1$ emission line.[30] However, MHz repetition rates make it possible to obtain count rates as high as those in conventional static experiments. In Figure 3, we present the first full $K\alpha$ and $K\beta$ spectra of photoexcited $[Fe(bipy)_3]^{2+}$, taken with a 3.26 MHz repetition rate at a delay of $\Delta t$ = 100 ps. The spectra are in good agreement with the static HS/LS spectra taken on a closely related spin-crossover compound ($[Fe(phen)_2(NCS)_2]$),[39] and they allow us to determine the average spin momentum of Fe or directly determine the HS fraction $\gamma$ using line shape analysis. In this paper, we use the approach called integrated absolute difference (IAD), which is performed by taking the absolute values of the difference between a sample and a reference spectrum and integrating them to obtain the IAD value. The IAD determined for the HS and LS spectra of appropriate reference materials can be referred to as $IAD_{HL}$, and the scaling factor between this and the IAD of a sample is the HS fraction, $IAD = \gamma IAD_{HL}$. The uncertainty of the IAD values can be readily calculated from the counting statistics using error propagation. This approach is explained in detail in ref 39 and has been used with success to


dx.doi.org/10.1021/jp306917x | J. Phys. Chem. A 2012, 116, 9878−9887

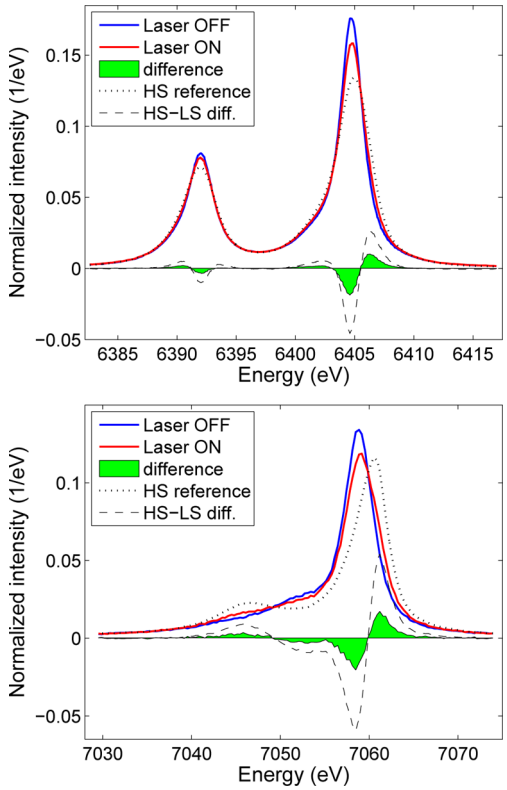


**Figure 3.** K$\alpha$ (top) and K$\beta$ (bottom) spectra of $[Fe(bipy)_3]^{2+}$ with $\Delta t$ = 100 ps for the laser-on data. The change from the LS state at laser excitation is evident, and by direct comparison with HS/LS reference spectra, accurate determination of the HS fraction $\gamma$ (close to 40% for this data set) can be determined from these spectra with very good S/N.

relate the spectral variations to spin state changes in many studies.[57−61] In the present work for the LS, we use an internal reference, the spectrum of the $[Fe(bipy)_3]^{2+}$ solution without laser excitation. The HS reference spectra were measured on a powder sample of $[Fe(phen)_2(NCS)_2]$ at room temperature. Figure 3 displays also the difference of the HS and LS reference spectra; the calculations behind the IAD method can be taken as finding the scaling factor between the sample difference spectrum and the HS−LS difference (displayed in Figure 3 as the green filled curve and dashed line, respectively). The IAD approach is very compatible with our data acquisition strategy of taking shot-by-shot alternating ground-state (laser-off, i.e., LS reference) and laser-on data at chosen delays. Typical values for the maximum HS fraction, here referred to as $\gamma_0$, were between 30 and 40%, depending on particular experimental parameters, such as spatial overlap of the X-ray and laser beams.

**Difference Scattering Signatures of the Excited-State Structures.** Figure 4 shows the acquired difference scattering signals for the six investigated time delays with $\Delta t \geq 100$ ps. The difference signals are each constructed from 134 on/off pairs of images with a 10 s integration time, azimuthally integrated and scaled to a known standard (water[62]). It is worth noting that for all time delays, the $\Delta S/S$ ratio is less than $10^{-3}$, highlighting the need for the high repetition rate. The time delays were chosen to fully cover the lifetime of the excited HS state of $[Fe(bipy)_3]^{2+}$ ($\tau$ = 665 ps[55]).

Qualitative inspection of this set of difference curves reveals a negative feature at low Q that decays on a time scale of several hundred picoseconds and an oscillatory feature from $Q$ = 1.5 to

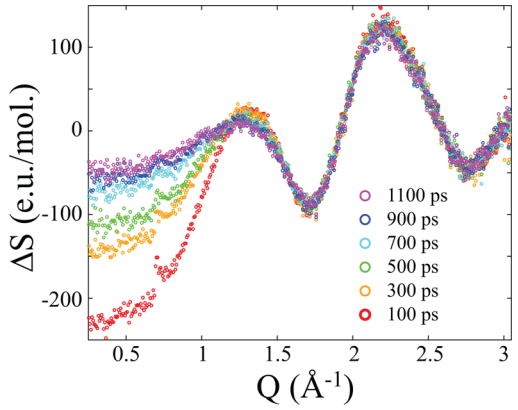


**Figure 4.** Averaged difference signals for 134 on/off repetitions at six time delays following the photoexcitation event at $\Delta t$ = 0 ps. The signal is dominated by a negative feature at low Q related to the expansion of the solute molecule and an oscillatory feature arising from the changes in the bulk structure of the solvent (water).

3 Å$^{-1}$, which appears to be essentially constant for all of the investigated time delays. The negative feature in the low-Q region can be directly associated with the well-established[56,63] 0.2 Å elongation of the Fe−N bond in excited-state $[Fe(bipy)_3]^{2+}$. This feature and its observed dynamic time scale constitute an unambiguous scattering signature from the light-triggered formation of HS $[Fe(bipy)_3]^{2+}$ molecules with the excited-state structure. The oscillatory feature at around $Q$ = 2 Å$^{-1}$ arises from changes in the intermolecular structure of the bulk solvent, as discussed in detail below.

**Comparison of XAS/XES/XDS-Measured Kinetics.** The strong and prompt XAS response to photoexcitation was utilized to optimize the experimental conditions (notably, the overlap of the two beams in space and time), so that they were appropriate for studying the structural and electronic dynamics of the $[Fe(bipy)_3]^{2+}$. In the XANES spectrum, the 7125 eV feature shows the largest change following the spin transition. Figure 5a displays the time evolution of the intensity of this signal feature, which corresponds to the formation and decay of the HS state. The width of the rise centered at $\Delta t$ = 0 corresponds to the X-ray probe pulse width, while the later exponential decay is governed by the lifetime of the HS state. This time evolution is fitted by an expression of the form

$$I(\Delta t) = I(t - t_0) = \gamma_0 \int_{-\infty}^{\infty} \frac{1}{\sigma\sqrt{2\pi}} e^{-y^2/2\sigma^2} H(t - t_0 - y) \, e^{-(t-t_0-y)/\tau} \, dy \quad (1)$$

derived from a Gaussian broadening (with width $\sigma$) of an exponential decay starting at $t_0$ with starting value $\gamma_0$, here interpreted as the photoexcitation (HS) fraction just after laser excitation. The $\tau$ stands for the lifetime of the HS state and $H$ is the heaviside step function. Key parameters for each data set are listed in Table 1, and we note that for all three methods, the lifetime of the HS state is found to be in reasonable agreement with the lifetimes found in previous studies.[6] Also, the expected ~80 ps X-ray probe pulse width for APS in the 24-bunch mode is well reproduced between methods.

The simultaneous utilization of scattering and spectroscopy techniques allows us to follow the dynamics on both the local and a more extended range. XES is practically sensitive to the


dx.doi.org/10.1021/jp306917x | J. Phys. Chem. A 2012, 116, 9878−9887

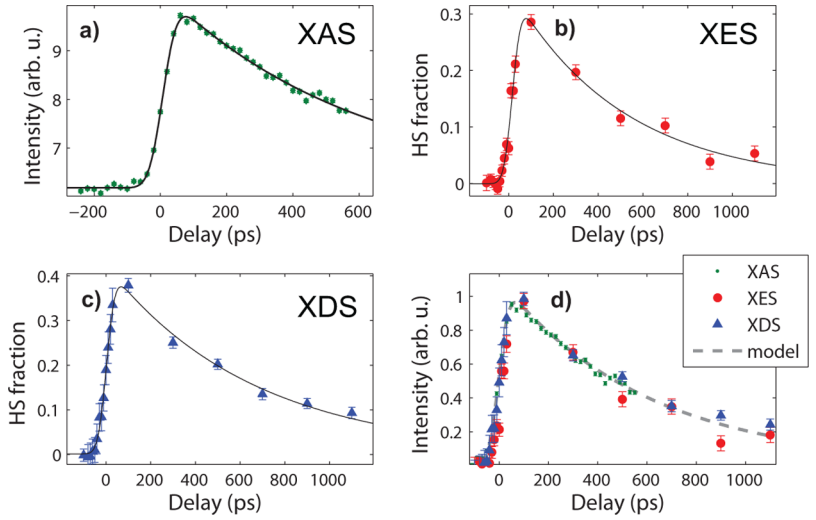


**Figure 5.** Time evolution of the HS fraction from (a) XAS, (b) XES, and (c) XDS, independently fitted with eq 1. The data in (a) were taken in a separate measurement, while the data in (b) and (c) were taken simultaneously. A unified plot of the results from the three techniques is seen in (d), highlighting how the observed dynamics are fully consistent between techniques as well as individual experiments.

**Table 1. Parameter Estimates Obtained by Fitting Equation 1 to the XAS, XES, and XDS Data Sets, With 95% Confidence Limits**[a]

| technique | lifetime ($\tau$) (ps) | fwhm pulse width (ps) | $t_0$ (ps) | $\gamma_0$ |
|---|---|---|---|---|
| XAS | 594 ± 30 | 78 ± 6 | 9.2 ± 2 | n.a. |
| XES | 503 ± 100 | 71 ± 18 | 17.6 ± 6 | 0.34 ± 0.04 |
| XDS | 657 ± 75 | 71 ± 16 | 4.2 ± 5 | 0.43 ± 0.03 |

[a]In general, good agreement between the three measurements is observed but with a tendency for the XES results to exhibit a slightly shorter lifetime.

changes on the $Fe^{2+}$ ion only. From such measurements, the relative amount of excited complexes in the probed volume, the HS fraction, can be obtained from the laser-on/laser-off XES difference spectra at different delays. The HS fraction plotted against the delay reveals the spin state dynamics; see Figure 5b. The continuous line is a fitted model curve that corresponds to the above equation, and the fit parameters are listed in Table 1. Note that $\gamma_0$ also becomes relevant here as XES quantitatively determines the HS fraction. Therefore, this fit parameter is the HS conversion yield (initial HS population); the best-fit results correspond to an initial HS fraction of 0.34 ± 0.04. The lifetime of the HS state compares moderately well with that obtained from XAS.

To quantify the dynamics of the set of the difference scattering signals, each individual difference signal $\Delta S(Q,\Delta t)$ was considered to be a combination of contributions from changes in the structure of the solute and from changes in bulk solvent scattering due to changes in solvent temperature $T$ and density $\rho$[19,44]

$$\Delta S(Q)_{\Delta t} = \gamma_{\Delta t}\Delta S(Q)_{\text{Solute}} + \Delta T_{\Delta t}\left.\frac{\partial(\Delta S(Q))}{\partial T}\right|_{\rho} + \Delta\rho_{\Delta t}\left.\frac{\partial(\Delta S(Q))}{\partial \rho}\right|_{T} \quad (2)$$

where the subscript $\Delta t$ denotes dependence on the time delay. The simulated solute contribution $\Delta S(Q)_{\text{Solute}}$ was calculated by a combined approach utilizing both DFT-derived structures and molecular dynamics (MD) simulations. We used the molecular structures for the LS and the HS states calculated by Daku and Hauser using an ab initio molecular dynamics (AIMD) approach with water as the solvent.[63] The structures determined in their study were then introduced into classical MD simulations with 4171 water molecules (OPLS2005 force field with the TIP4P water model), which were then allowed to evolve at constant $T$ and $\rho$ for 2000 ps with a 2 fs step size and with the structure of the solute held rigid by imposing constraints on all $[Fe(bipy)_3]^{2+}$ bonds. From two ensembles (with either HS or LS solute molecules) of such simulations, the average scattering was calculated for both model structures (including the surrounding solvent) using the Debye equation to finally yield $\Delta S(Q)_{\text{Solute}} = \Delta S(Q)^{\text{model}}_{\text{HS}} - \Delta S(Q)^{\text{model}}_{\text{LS}}$. This combined approach allowed direct incorporation of local changes in scattering due to changes in solvation and excluded volume effects following the photoinduced change in the solute structure and improved the quality of the fits very significantly compared to only incorporating the structural changes in the solute.

Fitting eq 2 to the measured $[Fe(bipy)_3]^{2+}$ $\Delta S$ signals, Figure 5c shows the fitted excitation fraction $\gamma_{\Delta t}$ as a function of time delay. The good agreement observed between the three methods is illustrated in Figure 5d, and Table 1 reports key experimental parameters obtained by fitting eq 1 to each data set. The same kinetics are observed with all methods, and the small discrepancy in excitation fractions observed with XDS and XES is attributed to uncertainties in accurate scaling of the XDS data set due to the significant air scattering. In the fit process, strong correlation between $\Delta\rho$ and $\Delta T$ was observed and led to unstable fits for some time delays. This was handled by the reasonable assumption of a monotonically increasing transient temperature change (within the error bars).

Figure 6(left) shows the good agreement between the measured $\Delta S$ and the best-fit simulated signals; for clarity of presentation, only data points with $\Delta t \geq 0$ ps are shown. The right panel of Figure 6 shows the relative contributions from each of the three signals included in the model calculations. An immediate grow-in of all three components is observed, followed by a decrease in the contributions from structural changes in the solute and from changes in the density of the


dx.doi.org/10.1021/jp306917x | J. Phys. Chem. A 2012, 116, 9878−9887

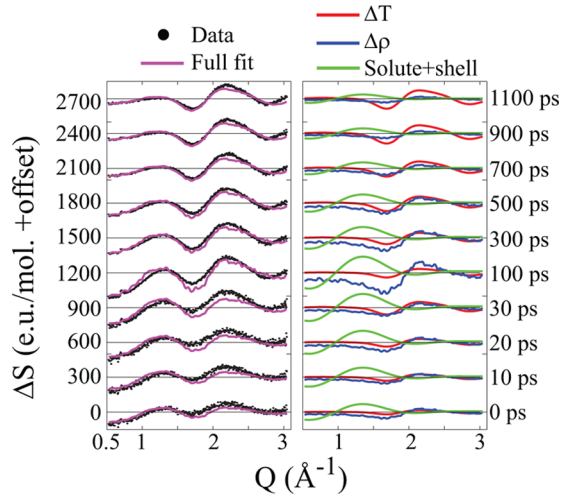


**Figure 6.** (Left) Data (black points) and fits (purple lines) for all time delays with $\Delta t \geq 0$ ps. Noise on the fit traces is due to the noise in the experimentally determined differential $[\partial(\Delta S)/\partial\rho]|_T$. (Right) The three contributions to the best-fit difference signals for each time delay. Green traces arise from changes in structure and solvation of $[Fe(bipy)_3]^{2+}$, red traces are from heating of the solvent, and blue traces arise from changes in the bulk density of the solvent.

solvent. The time scale for this decrease matches the 665 ps lifetime of the HS state of $[Fe(bipy)_3]^{2+}$ and is accompanied by a further increase in the temperature of the solvent.

Quantifying these general observations, Figure 7 shows the magnitude of each of the three components of the fits

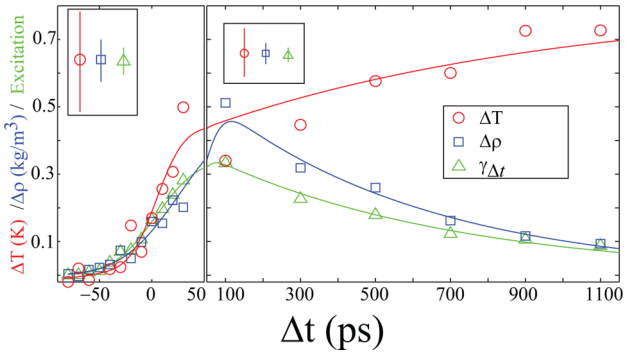


**Figure 7.** Time evolution of the magnitude of each of the three contributions to the total difference signal. A fast grow-in is observed for $\Delta t$ < 100 ps for all three parameters. On time scales longer than $\Delta t$ = 100 ps, the temperature is observed to rise further, whereas the density and excitation contributions are observed to decay on the time scale of the HS state of $[Fe(bipy)_3]^{2+}$, in full agreement with the model discussed in the text. The top-left insets illustrate the error bars (95% C.L.) for the fit parameters in the two regions.

presented in Figure 6 as a function of $\Delta t$. The behavior of these three contributions, which together describe the structural evolution of the investigated sample volume following photoexcitation, is essentially the same on the $\Delta t$ < 50 ps time scale for all three but diverges for $\Delta t$ > 50 ps.

Turning first to the fastest time scales, the common response is fully explained by a stepwise change due to the (short) excitation laser pulse, broadened by the finite width of the X-ray probe pulse, as described in detail above. On the longer time scales, the density change of the bulk solvent ($\Delta_\rho$) is observed to follow the same exponential decay as the HS fraction $\gamma_{\Delta t}$ and with a similar time constant, $\tau_{\Delta\rho}$ = 500 ± 150 ps and $\tau_\gamma$ = 660 ± 90 ps. The observed increase in temperature is well captured by the same broadened step function followed by an increase taking the form of an exponential grow-in but with a poorly determined time constant, $\tau_{\Delta T}$ = 910 ± 600 ps. These functional forms have been independently fitted to the three data series shown in Figure 7 and are shown as solid lines.

The temperature response of the solvent can be understood immediately from the decay processes previously described for $[Fe(bipy)_3]^{2+}$ as the majority of the absorbed photon energy is released very fast ($\tau \approx 1$ ps) as vibrational energy to the solvent after the ~130 fs intersystem crossing.[55] This is then followed by a slower release of energy as the HS state decays nonradiatively ($\tau \approx 665$ ps). On the time scales accessible to the present experiment, this results in a (broadened) step-like increase in temperature followed by the observed further increase on the time scale of the HS lifetime. The average ~0.5° temperature increase over the probed sample volume is in good agreement but somewhat larger than the corresponding values obtained in previous studies using kHz repetition schemes with higher pump pulse fluences.[19] The larger temperature increase is expected as the concentration of excited molecules is more than 10 times higher in the present experiment and the decay modes of $[Fe(bipy)_3]^{2+}$ are almost completely nonradiative, but it is still significantly less than the temperature increase observed to drive LS−HS conversion in the low-temperature crystal studies of Cailleau et al.[64] No such temperature-driven processes are expected for $[Fe(bipy)_3]^{2+}$ due to the large LS−HS energy difference, 0.74 eV.[55]

To understand the prompt increase in density on the 100 ps time scale, we turn to a key finding of the computational study of Daku and Hauser,[63] namely, the change in solvation of $[Fe(bipy)_3]^{2+}$ following conversion to the HS state. From their theoretical investigations, a consequence of the excitation and the structural change is the expulsion of ~2 water molecules from the solvation shell to the bulk solvent. With the characteristic time scale for mass transport out of the probed volume given by the Longaker−Litvak time $\tau_L = L/c$, with as the $L$ the pump pulse size and $c$ as the the speed of sound,[44] there is no time for mass transport out of the investigated volume on the 100 ps time scale. Thus, the proposed solvation change would be expected to lead to an increase in the density of the bulk solvent. For a 20 mM solution (2750 solvent molecules per solute) with 40% photoexcitation, a lower limit on the associated change in density can be very roughly estimated to be 0.4 × 2/2750 = 0.03%, excluding all other changes such as, for example, the increased volume of the solute and the reported reorientation of the first solvent shell. This lower limit of a 0.03% fractional change corresponds to a change in density of 0.3 kg/m$^3$ and agrees reasonably well with the value estimated from our data analysis, ~0.5 kg/m$^3$. However, to fully establish and quantify the proposed direct connection between the observed macroscopic change in density and the microscopic phenomenon of solvent shell reorganization, further studies are needed.

Whereas this analysis fully accounts for the qualitative features of the observed evolution of the measured difference signals, a few minor discrepancies in the quantitative results are present. First, the decay time determined for $\Delta T$ and $\Delta\rho$ are similar but not identical, and the increase in density measured is somewhat larger than would be expected from the simplest interpretation of the computational result. To address these issues, a second analysis was performed, where advantage was


dx.doi.org/10.1021/jp306917x | J. Phys. Chem. A 2012, 116, 9878−9887

taken of the independent measurement of the excitation fraction offered by the XES data. This allowed us to lock in the excitation fraction in the analysis, and through the significant correlations between this parameter and $\Delta\rho$, the uncertainty in determining the numeric value of $\Delta\rho$ for each time step was reduced by ~15%. The $\Delta_\rho$ value determined for each $\Delta t$ was lowered by ~10%, improving the agreement with the model prediction. Carrying these results over to the kinetic analysis, we find $\tau_{\Delta\rho} = 620 \pm 90$ ps, in much better agreement with both the present and previous results for $\tau_\gamma$

A second issue to address in the qualitative analysis is the (small) discrepancy between the rise time of the three components of the fit. Within the physical model established here, one would expect these to be identical and to be given by the width of the X-ray probe pulse. However, the temperature appears to rise slightly faster than the excitation fraction, and the change in density appears to rise slightly slower. Although $[Fe(bipy)_3]^{2+}$ in solution is known to be exceptionally robust to even prolonged and intense X-ray exposure, we tentatively suggest that during the ~12 h of exposure to the focused X-ray beam, a very small amount of degradation product capable of absorbing light at 532 nm and releasing the absorbed energy as heat is formed. This would lead to increased heat deposition by each pump pulse over the course of the experiment. In particular, the contribution from previous pump pulses would not be compensated for by the subtraction of only one background signal, and over the course of hours, the observed (transient) temperature increase would go up, and the observed (transient) density increase would diminish, as observed. Had the increased heating been due to changes in excitation fractions due to evaporative losses of solvent, we would expect to observe concomitant changes in the measured excitation fractions as the deposited energy from the laser-excited molecules and thus the solvent heating are linear functions of the excitation fraction. This is not observed.

The tentative suggestion of increased heat deposition due to a very small amount of decay product is further supported by a second analysis of the difference signals, where instead of one early ($\Delta t < -50$ ps) time delay being used as the background contribution, incremental difference patterns are calculated from successive time delays. Applying this analysis, the rise times are more in agreement, and we also obtain better fits to the $\Delta t < 100$ ps difference curves. However, due to the order in which the data for each time delay were acquired, this method cannot be applied to the entire data set.

A full investigation of the local solvation dynamics of photoexcited $[Fe(bipy)_3]^{2+}$ is beyond the scope of the present paper. However, the finding that such dynamics can be directly investigated by time-resolved XDS underscores the new possibilities opened up by increasing the available X-ray flux by 2−3 orders of magnitude, as well as the benefits of using a "tickle and probe" approach, where smaller laser fluences are used for the pump pulse, thus not drowning out small signals by large thermal effects.

## CONCLUSIONS

In the present study, we have utilized the recently developed MHz laser pump/X-ray probe capability[32] of the 7ID beamline at the Advanced Photon Source to combine the complementary and photon-hungry techniques of X-ray emission spectroscopy and X-ray diffuse scattering in a single experiment. Even though the single-pulse energy of the laser pump pulses is limited to the <10 $\mu$J regime for MHz repetition rates, tight focusing (<100 $\mu$m) of both beams allowed us to obtain high excitation fractions (30−40% HS $[Fe(bipy)_3]^{2+}$) in the probed sample volume. The 3.26 MHz repetition rate of the experiment is the highest reported yet and led to an increase in usable X-ray flux on the sample by 3 orders of magnitude compared to the usual kHz synchrotron-based time-resolved experiments. This rendered both techniques fully feasible and gave XES data quality comparable to that of steady-state experiments. The increase in flux and the experimental design also allowed simultaneous collection of high-quality scattering data for this comparatively light compound in only a few hours. By combining the XES data with XDS results, the presence of the high-spin configuration of the $Fe^{II}$ ion could be unambiguously tied to the global structural changes in molecular structure observed directly in the $\Delta S$ signals. The direct and simultaneous measurement of the excited-state fraction was used to significantly reduce the uncertainties, directly addressing complications with strongly correlated fit parameters, as suggested in previous work.[45] The combined experiment thus offers benefits beyond that of simply combining information from two separate experiments, in addition to the highly efficient use of the X-ray beam.

The superior quality of the scattering data combined with the comparatively gentle laser excitation further allowed us to tentatively confirm a key prediction of recent theoretical work on $[Fe(bipy)_3]^{2+}$.[63] By quantitative analysis of the subnanosecond response of the bulk solvent structure, the consequences of the solvation dynamics of the HS $[Fe(bipy)_3]^{2+}$ were detected by monitoring the increase in solvent density due to expulsion of water molecules from the first solvation shell following photoexcitation.

Even as $[Fe(bipy)_3]^{2+}$ is a thoroughly studied model compound in time-resolved science, this experimental detection of a process involving only the disordered rearrangement of light elements highlights how the much increased X-ray flux will allow future time-resolved experiments to move from molecular systems tailored or chosen to match the usually low X-ray intensity and to move on to more general classes of systems that have so far only been studied with steady-state methods.

## AUTHOR INFORMATION

### Corresponding Author

*E-mail: hald@fysik.dtu.dk (K.H.); vanko@rmki.kfki.hu (G.V.).

### Notes

The authors declare no competing financial interest.

## ACKNOWLEDGMENTS

This project was supported by the European Research Council via Contract ERC-StG-259709, by the Danish National Research Foundation's Centre for Molecular Movies, by the European XFEL, and DANSCATT. A.M.M., G.D., S.H.S., E.P.K., and L.Y. acknowledge support from the U.S. Department of Energy (DOE) Office of Science, Division of Chemical, Geological and Biological Sciences, under Contract No. DE-AC02-06CH11357. K.H. gratefully acknowledges support from the Carlsberg and Villum Foundations. G.V. acknowledges support from the Bolyai János Fellowship of the Hungarian Academy of Sciences. V.S. acknowledges support from the European Research Council, Advanced Investigator Grant, VISCHEM-226136. S.E.C. gratefully acknowledges funding from the Swedish Research Council. C.B., A.G. and W.G. acknowledge funding from the German Research Association

DFG via SFB925 (project A4). Use of the Advanced Photon Source, an Office of Science User Facility operated for DOE Office of Science by Argonne National Laboratory, was supported by the U.S. DOE under Contract No. DE-AC02-06CH11357.

## REFERENCES

(1) Fleming, G. R.; Cho, M. *Annu. Rev. Phys. Chem.* **1996**, *47*, 109−134.
(2) Ball, P. *Chem. Rev.* **2008**, *108*, 74−108.
(3) Zhong, D.; Pal, S. K.; Zewail, A. H. *Chem. Phys. Lett.* **2011**, *503*, 1−11.
(4) Cramer, C.; Truhlar, D. *Chem. Rev.* **1999**, *99*, 2161−2200.
(5) Bressler, C.; Milne, C.; Pham, V.-T.; ElNahhas, A.; van der Veen, R. M.; Gawelda, W.; Johnson, S.; Beaud, P.; Grolimund, D.; Kaiser, M.; Borca, C. N.; Ingold, G.; Abela, R.; Chergui, M. *Science* **2009**, *323*, 489−492.
(6) Cannizzo, A.; Milne, C.; Consani, C.; Gawelda, W.; Bressler, C.; van Mourik, F.; Chergui, M. *Coord. Chem. Rev.* **2010**, *254*, 2677−2686 ; 18th International Symposium on the Photochemistry and Photophysics of Coordination Compounds Sapporo, 2009..
(7) Lindenberg, A.; Kang, I.; Johnson, S.; Missalla, T.; Heimann, P.; Chang, Z.; Larsson, J.; Bucksbaum, P.; Kapteyn, H.; Padmore, H.; Lee, R.; Wark, J.; Falcone, R. *Phys. Rev. Lett.* **2000**, *84*, 111−114.
(8) Chen, L.; Jager, W.; Jennings, G.; Gosztola, D.; Munkholm, A.; Hessler, J. *Science* **2001**, *292*, 262−264.
(9) Techert, S.; Schotte, F.; Wulff, M. *Phys. Rev. Lett.* **2001**, *86*, 2030−2033.
(10) Schotte, F.; Lim, M.; Jackson, T.; Smirnov, A.; Soman, J.; Olson, J.; Phillips, G.; Wulff, M.; Anfinrud, P. *Science* **2003**, *300*, 1944−1947.
(11) Collet, E.; Lemee-Cailleau, M.; Buron-Le Cointe, M.; Cailleau, H.; Wulff, M.; Luty, T.; Koshihara, S.; Meyer, M.; Toupet, L.; Rabiller, P.; Techert, S. *Science* **2003**, *300*, 612−615.
(12) Johnson, S.; Heimann, P.; Lindenberg, A.; Jeschke, H.; Garcia, M.; Chang, Z.; Lee, R.; Rehr, J.; Falcone, R. *Phys. Rev. Lett.* **2003**, *91*, 157403.
(13) Saes, M.; Bressler, C.; Abela, R.; Grolimund, D.; Johnson, S.; Heimann, P.; Chergui, M. *Phys. Rev. Lett.* **2003**, *90*, 047403.
(14) Ihee, H.; Lorenc, M.; Kim, T.; Kong, Q.; Cammarata, M.; Lee, J.; Bratos, S.; Wulff, M. *Science* **2005**, *309*, 1223−1227.
(15) Gawelda, W.; Bressler, C.; Saes, M.; Kaiser, M.; Tarnovsky, A. N.; Grolimund, D.; Johnson, S. L.; Abela, R.; Chergui, M. *Phys. Scr.* **2005**, *T115*, 102−106.
(16) Gawelda, W.; Johnson, M.; de Groot, F.; Abela, R.; Bressler, C.; Chergui, M. *J. Am Chem. Soc.* **2006**, *128*, 5001−5009.
(17) Hertlein, M.; Adaniya, H.; Amini, J.; Bressler, C.; Feinberg, B.; Kaiser, M.; Neumann, N.; Prior, M.; Belkacem, A. *Phys. Rev. A* **2006**, *73*, 062715.
(18) Cammarata, M.; Levantino, M.; Schotte, F.; Anfinrud, P. A.; Ewald, F.; Choi, J.; Cupane, A.; Wulff, M.; Ihee, H. *Nat. Methods* **2008**, *5*, 881−886.
(19) Christensen, M.; Haldrup, K.; Bechgaard, K.; Feidenhans'l, R.; Kong, Q.; Cammarata, M.; Russo, M. L.; Wulff, M.; Harrit, N.; Nielsen, M. M. *J. Am. Chem. Soc.* **2009**, *131*, 502−508.
(20) van der Veen, R. M.; Milne, C. J.; El Nahhas, A.; Lima, F. A.; Pham, V.-T.; Best, J.; Weinstein, J. A.; Borca, C. N.; Abela, R.; Bressler, C.; Chergui, M. *Angew. Chem., Int. Ed.* **2009**, *48*, 2711−2714.
(21) Haldrup, K.; Harlang, T.; Christensen, M.; Dohn, A.; van Driel, T. B.; Kjær, K. S.; Harrit, N.; Vibenholt, J.; Guerin, L.; Wulff, M.; Nielsen, M. M. *Inorg. Chem.* **2011**, *50*, 9329−9336.
(22) Fornuier, B.; Coppens, P. *J. Synchrotron Radiat.* **2012**, *19*, 497−502.
(23) Khalil, M.; Marcus, M. A.; Smeigh, A. L.; McCusker, J. K.; Chong, H. H. W.; Schoenlein, R. W. *J. Phys. Chem. A* **2006**, *110*, 38−44.
(24) Elles, C. G.; Shkrob, I. A.; Crowell, R. A.; Arms, D. A.; Landahl, E. C. *J. Chem. Phys.* **2008**, *128*, 061102.
(25) Huse, N.; Kim, T. K.; Jamula, L.; McCusker, J. K.; de Groot, F. M. F.; Schoenlein, R. W. *J. Am. Chem. Soc.* **2010**, *132*, 6809−6816.
(26) Huse, N.; Cho, H.; Hong, K.; Jamula, L.; de Groot, F. M. F.; Kim, T. K.; McCusker, J. K.; Schoenlein, R. W. *J. Phys. Chem. Lett.* **2011**, *2*, 880−884.
(27) Van Kuiken, B. E.; Huse, N.; Cho, H.; Strader, M. L.; Lynch, M. S.; Schoenlein, R. W.; Khalil, M. *J. Phys. Chem. Lett.* **2012**, *3*, 1695−1700.
(28) Harpham, M. R.; et al. *Angew. Chem., Int. Ed.* **2012**, *51*, 7692−7696.
(29) Stern, E. A.; Brewe, D. L.; Beck, K. M.; Heald, S. M.; Feng, Y. *Phys. Scr.* **2005**, *T115*, 1044−1046.
(30) Vankó, G.; Glatzel, P.; Pham, V.-T.; Abela, R.; Grolimund, D.; Borca, C. N.; Johnson, S. L.; Milne, C. J.; Bressler, C. *Angew. Chem., Int. Ed.* **2010**, *49*, 5910−5912.
(31) Bressler, C.; Chergui, M. *Chem. Rev.* **2004**, *104*, 1781−1812.
(32) March, A. M.; Stickrath, A.; Doumy, G.; Kanter, E. P.; Krässig, B.; Southworth, S. H.; Attenkofer, K.; Kurtz, C. A.; Chen, L. X.; Young, L. *Rev. Sci. Instrum.* **2011**, *82*, 073110.
(33) Lima, F. A.; et al. *Rev. Sci. Instrum.* **2011**, *82*, 063111.
(34) Vanko, G.; et al. *J. Electron Spectrosc. Relat. Phenom.* **2012**, Accepted.
(35) Young, L.; Arms, D. A.; Dufresne, E. M.; Dunford, R. W.; Ederer, D. L.; Hohr, C.; Kanter, E. P.; Krassig, B.; Landahl, E. C.; Peterson, E. R.; Rudati, J.; Santra, R.; Southworth, S. H. *Phys. Rev. Lett.* **2006**, *97*, 083601.
(36) Glatzel, P.; Bergmann, U. *Coord. Chem. Rev.* **2005**, *249*, 65−95.
(37) Lee, N.; Petrenko, T.; Bergmann, U.; Neese, F.; DeBeer, S. *J. Am. Chem. Soc.* **2010**, *132*, 9715−9727.
(38) Wang, X.; de Groot, F. M. F.; Cramer, S. P. *Phys. Rev. B* **1997**, *56*, 4553−4564.
(39) Vankó, G.; Neisius, T.; Molnár, G.; Renz, F.; Kárpáti, S.; Shukla, A.; de Groot, F. M. F. *J. Phys. Chem. B* **2006**, *110*, 11647−11653.
(40) de Groot, F. M. F. *Chem. Rev.* **2001**, *101*, 1779−1808.
(41) Rueff, J. P.; Shukla, A.; Kaprolat, A.; Krisch, M.; Lorenzen, M.; Sette, F.; Verbeni, R. *Phys. Rev. B* **2001**, *63*, 132409.
(42) Badro, J.; Fiquet, G.; Guyot, F.; Rueff, J.-P.; Struzhkin, V. V.; Vankó, G.; Monaco, G. *Science* **2003**, *300*, 789−791.
(43) Lin, J.-F.; Vankó, G.; Jacobsen, S. D.; Iota, V.; Struzhkin, V. V.; Prakapenka, V. B.; Kuznetsov, A.; Yoo, C.-S. *Science* **2007**, *317*, 1740−1743.
(44) Cammarata, M.; Lorenc, M.; Kim, T.; Lee, J. H.; Kong, Q. Y.; Pontecorvo, E.; Russo, M. L.; Schiro, G.; Cupane, A.; Wulff, M.; Ihee, H. *J. Chem. Phys.* **2006**, *124*, 1245041−9.
(45) Haldrup, K.; Christensen, M.; Nielsen, M. M. *Acta Crystallogr., Sect. A* **2010**, *A66*, 261−260.
(46) Haldrup, K.; Christensen, M.; Cammarata, M.; Kong, Q.; Wulff, M.; Mariager, S. O.; Bechgaard, K.; Feidenhans'l, R.; Harrit, N.; Nielsen, M. M. *Angew. Chem., Int. Ed.* **2009**, *48*, 4180−4184.
(47) Kim, T. K.; Lee, J. H.; Wulff, M.; Kong, Q.; Ihee, H. *ChemPhysChem* **2009**, *10*, 1958−1980.
(48) Salassa, L.; Borfecchia, E.; Ruiu, T.; Garino, C.; Gianolio, D.; Gobetto, R.; Sadler, P. J.; Cammarata, M.; Wulff, M.; Lamberti, C. *Inorg. Chem.* **2010**, *49*, 11240−11248.
(49) Haldrup, K.; Harlang, T.; Christensen, M.; Dohn, A.; van Driel, T. B.; Kjaer, K. S.; Harrit, N.; Vibenholt, J.; Guerin, L.; Wulff, M.; Nielsen, M. M. *Inorg. Chem.* **2011**, *50*, 9329−9336.
(50) Kong, Q.; Kjaer, K. S.; Haldrup, K.; Sauer, S. P. A.; van Driel, T. B.; Christensen, M.; Nielsen, M. M.; Wulff, M. *Chem. Phys.* **2012**, *393*, 117−122.
(51) Press, W. H.; Flannery, B. P.; Teukolsky, T. A.; Vetterling, W. T. *Numerical Recipes — The Art of Scientific Computing*; Cambridge University Press: New York, 1986.
(52) Jun, S.; Lee, J. H.; Kim, J.; Kim, J.; Kim, K. H.; Kong, Q.; Kim, T. K.; Lo Russo, M.; Wulff, M.; Ihee, H. *Phys. Chem. Chem. Phys.* **2010**, *12*, 11536−11547.
(53) Dufresne, E. M.; Adams, B.; Arms, D. A.; Chollet, M.; Landahl, E. C.; Li, Y.; Walko, D. A.; Wang, J. *AIP Conf. Proc.* **2010**, *1234*, 181−184.

(54) Ejdrup, T.; Lemke, H. T.; Haldrup, K.; Nielsen, T. N.; Arms, D. A.; Walko, D. A.; Miceli, A.; Landahl, E. C.; Dufresne, E. M.; Nielsen, M. M. *J. Synchrotron Radiat.* **2009**, *16*, 387−390.
(55) Gawelda, W.; Cannizzo, A.; Pham, V.-T.; vanMourik, F.; Bressler, C.; Chergui, M. *J. Am. Chem. Soc.* **2007**, *129*, 8199−8206.
(56) Gawelda, W.; Pham, V.-T.; Benfatto, M.; Zaushitsyn, Y.; Kaiser, M.; Grolimund, D.; Johnson, S. L.; Abela, R.; Hauser, A.; Bressler, C.; Chergui, M. *Phys. Rev. Lett.* **2007**, *98*, 057401.
(57) Vankó, G.; de Groot, F. M. F. *Phys. Rev. B* **2007**, *75*, 177101.
(58) Sikora, M.; Knizek, K.; Kapusta, C.; Glatzel, P. *J. Appl. Phys.* **2008**, *103*, 07C907.
(59) Yamaoka, H.; Tsujii, N.; Oohashi, H.; Nomoto, D.; Jarrige, I.; Takahiro, K.; Ozaki, K.; Kawatsura, K.; Takahashi, Y. *Phys. Rev. B* **2008**, *77*, 115201.
(60) Herrero-Martin, J.; Mirone, A.; Fernandez-Rodriguez, J.; Glatzel, P.; Garcia, J.; Blasco, J.; Geck, J. *Phys. Rev. B* **2010**, *82*, 075112.
(61) Mao, Z.; Lin, J. F.; Jacobs, C.; Watson, H. C.; Xiao, Y.; Chow, P.; Alp, E. E.; Prakapenka, V. B. *Geophys. Res. Lett.* **2010**, *37*, L22304.
(62) Hura, G.; Sorenson, J.; Glaeser, R.; Head-Gordon, T. *J. Chem. Phys.* **2000**, *113*, 9140−9148.
(63) Daku, L. M. L.; Hauser, A. *J. Phys. Chem. Lett.* **2010**, *1*, 1830−1835.
(64) Cailleau, H.; Lorenc, M.; Guérin, L.; Servol, M.; Collet, E.; Buron-Le Cointe, M. *Acta Crystallogr., Sect. A* **2010**, *66*, 189−197.